fire

MDPI

Article

On Disintegrating Lean Hydrogen Flames in Narrow Gaps

Jorge Yanez [1], Leonid Kagan [2,*], Mike Kuznetsov [1] and Gregory Sivashinsky [2]

[1] Institute for Thermal Energy Technology and Safety (ITES), Karlsruhe Institute of Technology (KIT), Hermann-von-Helmholtz-Platz 1, 76344 Eggenstein-Leopoldshafen, Germany; jorge.yanez@kit.edu (J.Y.); mike.kuznetsov@kit.edu (M.K.)

[2] School of Mathematical Sciences, Tel Aviv University, Tel Aviv 6997801, Israel; grishas@tauex.tau.ac.il

* Correspondence: kaganleo@tauex.tau.ac.il

Abstract

The disintegration of near-limit flames propagating through the gap of Hele–Shaw cells has recently become a subject of active research. In this paper, the flamelets resulting from the disintegration of the continuous front are interpreted in terms of the Zeldovich flame balls stabilized by volumetric heat losses. A complicated free-boundary problem for 2D self-drifting near circular flamelets is reduced to a quasi-1D model. The quasi-1D formulation is then utilized to obtain the locus of the flamelet velocity, size, heat losses, and Lewis numbers at which the self-drifting flamelets may exist.

Keywords: hydrogen flames; diffusive-thermal instability; flame-balls

1. Introduction

Hydrogen flames have gained increasing attention over the last years as a clean and efficient energy solution [1]. Apart from their technological relevance, hydrogen flames are remarkably rich dynamically. Because of the high diffusion coefficient of molecular hydrogen, lean hydrogen–air flames are known to experience diffusive-thermal instability [2,3], manifesting themselves in the formation of a cellular structure in a state of chaotic self-motion. Moreover, as has recently been discovered by Veiga-López et al. [4], lean hydrogen–air flames evolving in narrow gaps of Hele–Shaw chambers and where heat loss effects become important, continuous cellular flames may disintegrate, forming self-drifting cup-like flamelets leaving tree-like or sprout-like traces (Figure 1).

Our Hele–Shaw cell, used to obtain the pictures in (Figure 1), was described in detail in [4,5]. The facility consists of two parallel 10 mm thick Plexiglas plates with a gap controlled by a hollow PVC frame of different thicknesses from 1 to 10 mm. The chamber in between the two plates is bounded by a PVC frame at three of its sides, while one of the short ones remains open. The chamber can be oriented vertically with an opening at the top or the bottom.

Hydrogen and air were mixed with two mass flow controllers to a certain concentration with an accuracy of $\pm 0.1\%H_2$. The quality of the mixture was checked using a gas analyzer. The mixture was ignited by an electric spark located on the open side. A time span of 500 ms between the opening of the cover and the ignition was provided to exclude the effect of vorticity and shear layers on the initial flame development. Pressure measurements and the Schlieren imaging procedure combined with a high-speed camera were used to monitor the structure and dynamics of the flame. The flame front and tail of the combustion products (such as water steam) were well resolved with the Schlieren system, as can be seen in (Figure 1).

check for updates

Academic Editor: Ali Cemal Benim

Received: 13 July 2025
Revised: 25 August 2025
Accepted: 27 August 2025
Published: 29 August 2025

Citation: Yanez, J.; Kagan, L.; Kuznetsov, M.; Sivashinsky, G. On Disintegrating Lean Hydrogen Flames in Narrow Gaps. *Fire* **2025**, *8*, 345. https://doi.org/10.3390/fire8090345

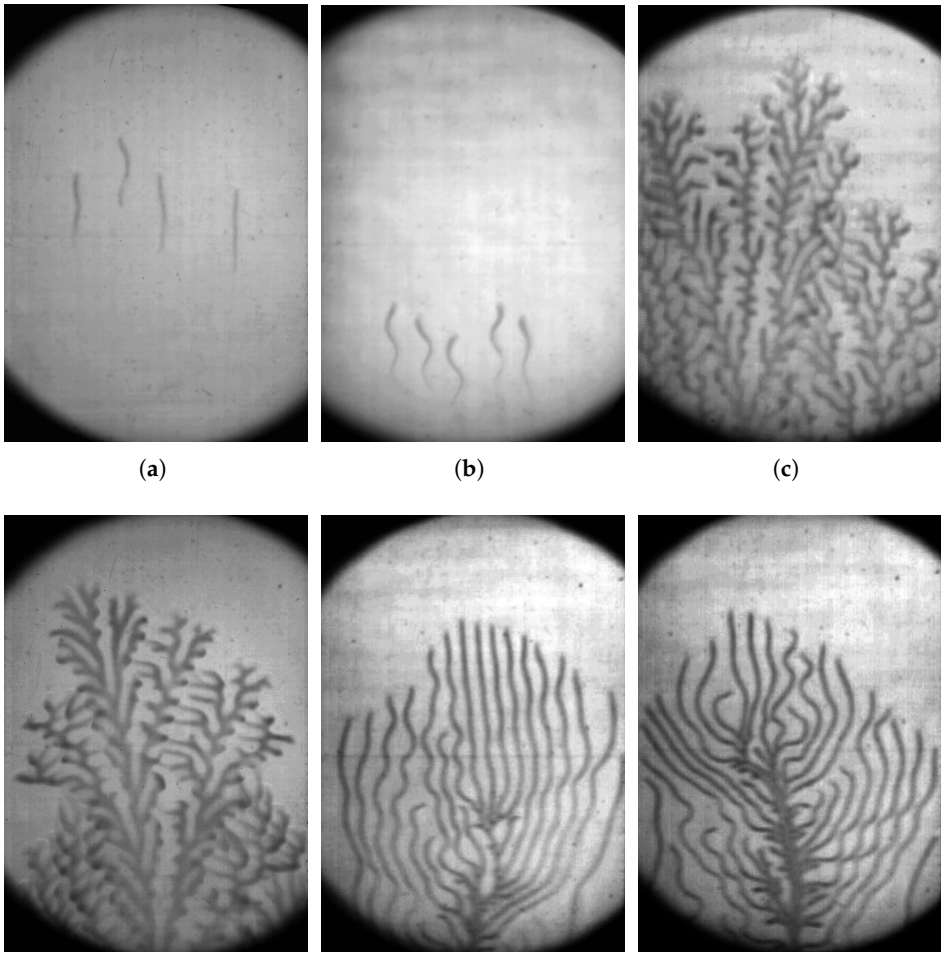

Figure 1. Hydrogen–air flamelets propagating through narrow gaps: (**a**) $d = 5$ mm, $\%H_2 = 5.0$; (**b**) $d = 3$ mm, $\%H_2 = 7.5$; (**c**) $d = 4$ mm, $\%H_2 = 7.0$; (**d**) $d = 5$ mm, $\%H_2 = 6.0$; (**e**) $d = 2$ mm, $\%H_2 = 9.75$; (**f**) $d = 2$ mm, $\%H_2 = 9.75$. Regimes: (**a**,**b**) one-headed finger, (**c**–**f**) one-headed branching.

These unexpected propagation modes extend flammability limits beyond those of the planar flames. This is particularly important for the safety studies of hydrogen-powered devices [6], as it implies that hydrogen flames may propagate in gaps much narrower than initially anticipated.

2. Reaction Diffusion Model

Some of the above features of the Hele–Shaw flames may be successfully captured by an ultra-simple constant-density, buoyancy-free, reaction diffusion model [7]. In suitably scaled variables and parameters, it reads

$$\frac{\partial T}{\partial t} = \frac{\partial^2 T}{\partial x^2} + \frac{\partial^2 T}{\partial y^2} + (1-\sigma)\Omega - q(T-\sigma), \tag{1}$$

$$\frac{\partial C}{\partial t} = \frac{1}{Le}\left(\frac{\partial^2 C}{\partial x^2} + \frac{\partial^2 C}{\partial y^2}\right) - \Omega, \tag{2}$$

$$\Omega = \frac{1}{2Le}(1-\sigma)^2 N^2 C \exp\left[N\left(1-\frac{1}{T}\right)\right], \tag{3}$$

where T is the temperature in units of T_b, the adiabatic temperature of combustion products; C is the concentration of the deficient reactant in units of C_0, its value in the fresh mixture;

x, y, t are the spatio-temporal coordinates in units of $\ell_{th} = D_{th}/U_b$ and ℓ_{th}/U_b, respectively; ℓ_{th} is the thermal width of the flame; U_b is the speed of a planar adiabatic flame; D_{th} is the thermal diffusivity of the mixture, $\sigma = T_0/T_b$, where T_0 is the temperature sustained at the walls of the Hele–Shaw cell; $Le = D_{th}/D_{mol}$ is the Lewis number; D_{mol} is the molecular diffusivity of the deficient reactant; $N = T_a/T_b$ is the scaled activation energy; T_a is the activation temperature; Ω is the appropriately normalized reaction rate to ensure that at large N, the scaled speed of the planar adiabatic flame is close to unity; q is the scaled heat loss intensity specified as $(\pi\ell_{th}/d)^2$; and d is the width of the Hele–shaw cell. The adopted expression for q stems from the 1D heat equation, $T_t = T_{zz}$, considered over the Hele–Shaw gap and subjected to isothermal boundary conditions, $T(z = \pm d/2\ell_{th}, t) = \sigma$. Hence, $T - \sigma \sim \exp\left[-(\pi\ell_{th}/d)^2 t\right] \cos\left[(\pi\ell_{th}/d)z\right]$. The exponential rate of the temperature decay is then extrapolated over the quasi-2D formulation of (1) and (2) in the (x, y) plane.

Figures 2 and 3 display the results of numerical simulations of the effect of heat loss on the breaking up of the flame in 2D.

Equations (1) and (2) are solved numerically by the finite difference method. Unknown T and C functions are resolved for fixed time increments inside of a rectangular area, $0 < x, y < 480$, on a uniform net. Spatial derivatives are approximated by second-order schemes. Temporal advance is calculated by the explicit Euler method of the first order.

For the simulations shown, the conditions $N = 10$, $Le = 0.25$, and $\sigma = 0.2$ were selected. Regarding heat loss, we have taken into account the following two hypotheses: (a) average heat losses, $q = 0.14$; (b) stronger heat losses, $q = 0.20$. Since this choice determines two different propagation velocities, the first condition required 740 dimensionless time units, whilst the second one required 1000.

As initial conditions, the radial temperature perturbation was selected:

$$T(x, y, 0) = \sigma + (1 - \sigma) \exp\left[-(x^2 + y^2)/\ell^2\right] \tag{4}$$

with $\ell = 0.25$. Fuel concentration was regarded as uniform, $C(x, y, 0) = 1$.

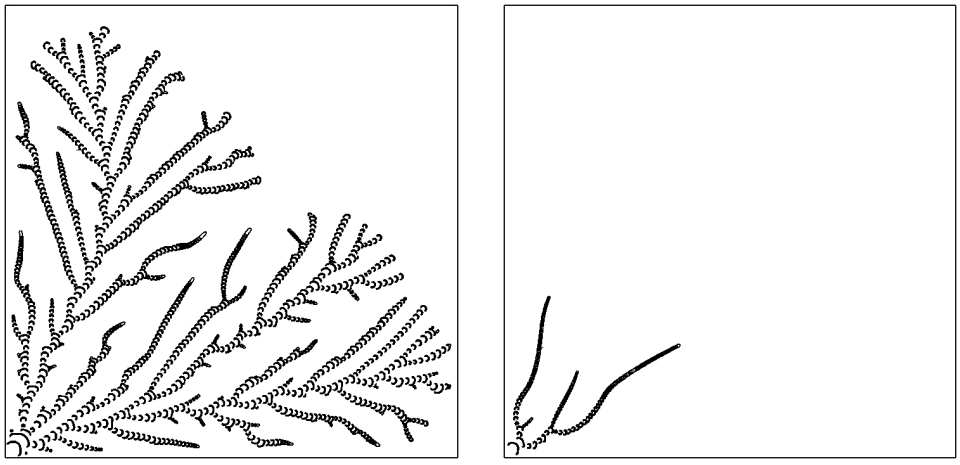

(**a**) (**b**)

Figure 2. Reaction rate $\Omega = 0.4$ at consecutive equi-spaced instants for one-headed flamelets under heat loss. (**a**) $q = 0.14$; (**b**) $q = 0.20$.

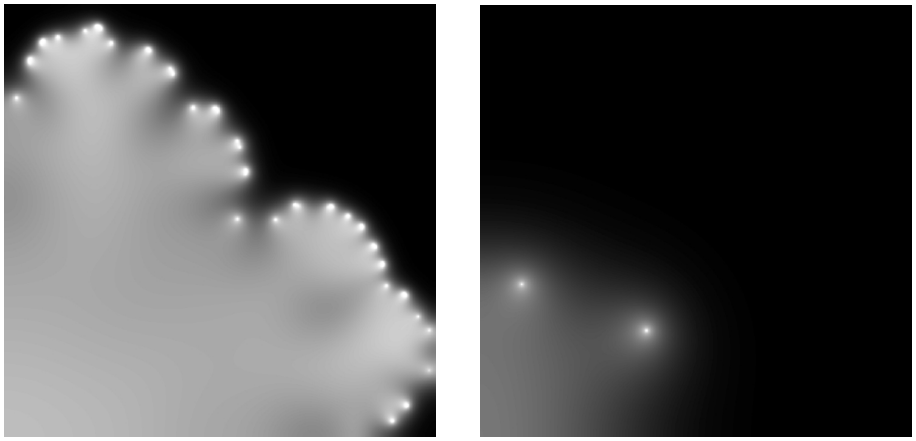

(**a**) (**b**)

Figure 3. Distribution of the deficient reactant concentration, C, at $t = 740$ (**a**) and $t = 1000$ (**b**). For conditions, see the legend for Figure 2. Lighter shading corresponds to lower concentration.

Near the quenching point, $q = 0.22$, higher heat loss leads to a lower drift velocity and smaller flamelet size (Figure 2), which is in line with experimental findings (Figures 4 and 5). Note that $q = 0.22$ significantly exceeds the quenching point $q = 0.018$ for the planar flame, with other conditions being identical (Figure 6).

A physically similar problem has also been numerically analyzed by Martínez-Ruiz et al. [8] and Dejoan [9]. These authors utilized large-scale numerical simulations of a model accounting both for the gas thermal expansion, buoyancy, and momentum loss.

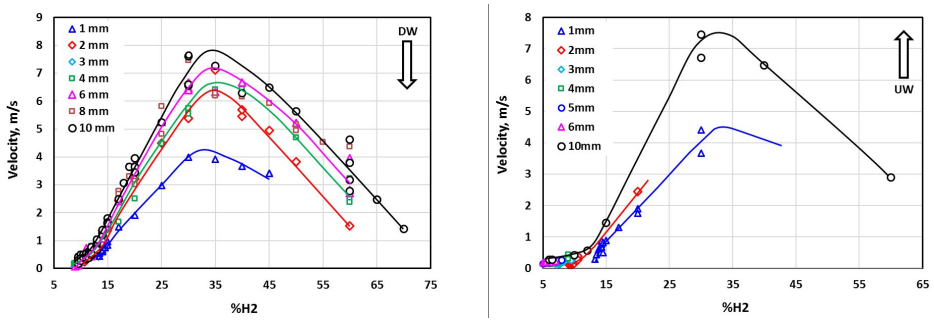

(**a**) (**b**)

Figure 4. Drift velocity for downward (DW) (**a**) and upward (UW) (**b**) propagation. See also Kuznetsov et al. [10] (Figure 7). The flame ball regime corresponds to ultra-lean flames ($\%H_2 < 20$).

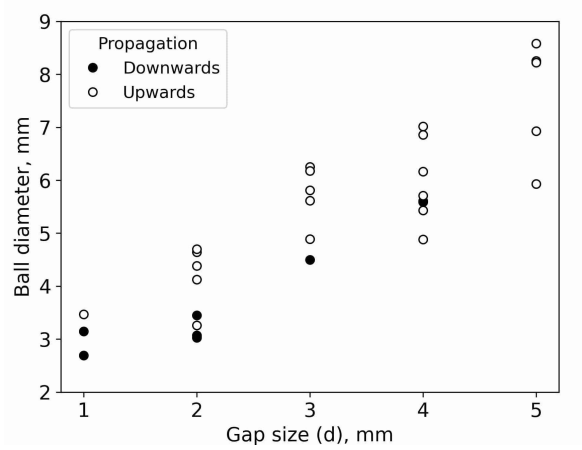

Figure 5. Flamelet diameter vs. gap size for one-headed flamelets.

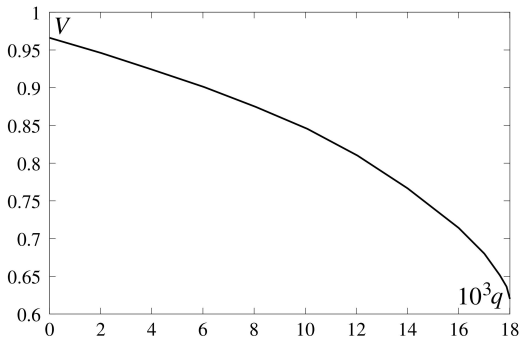

Figure 6. Drift velocity V vs. heat loss intensity q for a planar flame.

3. Reduction to a Free-Boundary Problem

The fingering patterns of Figures 1–3 are traces of self-drifting near-circular reactive spots. They may be regarded as a 2D version of familiar self-drifting 3D flame balls [11,12] (see also comment (ii) of Section 5). This observation in turn suggests the possible existence of individual self-drifting 2D flame balls described by time-independent reaction diffusion equations:

$$V\frac{\partial T}{\partial \eta} = \frac{\partial^2 T}{\partial \xi^2} + \frac{\partial^2 T}{\partial \eta^2} + (1-\sigma)\Omega - q(T-\sigma), \tag{5}$$

$$V\frac{\partial C}{\partial \eta} = \frac{1}{Le}\left(\frac{\partial^2 C}{\partial \xi^2} + \frac{\partial^2 C}{\partial \eta^2}\right) + (1-\sigma)\Omega, \tag{6}$$

which are subjected to boundary conditions

$$T(\xi^2+\eta^2 \to \infty) = \sigma,\ C(\xi^2+\eta^2 \to \infty) = 1. \tag{7}$$

$\xi = x$, $\eta = y + Vt$, and V is an eigenvalue of the problem. For theoretical analysis, it is technically advantageous to employ the familiar large-activation-energy $(N \gg 1)$ near-equidiffusive $(Le^{-1} - 1 \ll 1)$ approach, where the reaction diffusion system (5) and (6) is reduced to a free-boundary problem [13]. There, the reaction rate Ω transforms into a localized source distributed along the interface $\eta = R(\theta)\cos\theta$, $\xi = R(\theta)\sin\theta$. Equations (5) and (6) translate into the familiar set of equations for the reduced temperature Θ and excess enthalpy S:

$$V\frac{\partial \Theta^{(0)}}{\partial \eta} = \frac{\partial^2 \Theta^{(0)}}{\partial \xi^2} + \frac{\partial^2 \Theta^{(0)}}{\partial \eta^2}, \tag{8}$$

$$V\frac{\partial S}{\partial \eta} = \frac{\partial^2 \left(S - \alpha\Theta^{(0)}\right)}{\partial \xi^2} + \frac{\partial^2 \left(S - \alpha\Theta^{(0)}\right)}{\partial \eta^2} - \nu\Theta^{(0)} \tag{9}$$

where $\Theta = (T-\sigma)/(1-\sigma)$; $S = (\Theta + C - 1)\beta$; the Zeldovich number $\beta = (1-\sigma)N$ is assumed to be large; the Lewis number parameter, $\alpha = \left(Le^{-1} - 1\right)\beta$ and the re-scaled heat loss, $\nu = q\beta$, are assumed to be finite. Finally, $\Theta^{(0)}$ is the first coefficient of the re-scaled temperature for the asymptotic expansion on β, $\Theta^{(0)} = \Theta(\beta \to \infty)$.

At the reactive interface, $\xi^2 + \eta^2 = R^2(\theta)$, the following conditions are held:

$$[S]_-^+ = 0,\ \Theta^{(0)} = 1, \tag{10}$$

$$\left[\frac{\partial S}{\partial n}\right]_-^+ = \alpha\left[\frac{\partial \Theta^{(0)}}{\partial n}\right]_-^+, \tag{11}$$

$$\left[\frac{\partial \Theta^{(0)}}{\partial n}\right]_-^+ = -\left(1 + \frac{1}{R^2}\left(\frac{\partial R}{\partial \theta}\right)^2\right)^{1/2} \exp\left(\frac{S}{2}\right). \tag{12}$$

$\partial/\partial n$ is the normal derivative. And

$$\Theta^{(0)} \to 0,\ S \to 0, \tag{13}$$

at $\xi^2 + \eta^2 \to \infty$. Within the flame ball interface, the deficient reactant is assumed to be fully consumed:

$$C\left(\xi^2 + \eta^2 \le R^2(\theta)\right) = 0. \tag{14}$$

Finally, we observe that Equation (8) allows for the exact solution which in polar coordinates ($\eta = r\cos\theta, \xi = r\sin\theta$) reads [14,15]

$$\Theta^{(0)}(r,\theta) = \sum_m \exp(kr\cos\theta)\cos(m\theta)\cdot[A_m K_m(kr) + B_m I_m(kr)] + H. \tag{15}$$

K_m and I_m are modified Bessel functions of the first and second kind, $k = V/2$, and A_m, B_m, and H are parameters to be determined by conditions at $r = 0$, $r = \infty$, and $r = R(\theta)$.

4. Reduction to a Quasi-1D Model

4.1. General

The 2D free-boundary problem (8)–(14) is still too difficult for a straightforward analytical treatment. We therefore propose to consider its low-mode allocation-like reduction to a quasi-1D model that we believe will keep enough contact with the original 2D formulation. More specifically, in the quasi-1D approach, Θ, C, S are projected on the η-axis running through the center of the flame ball (Figure 7).

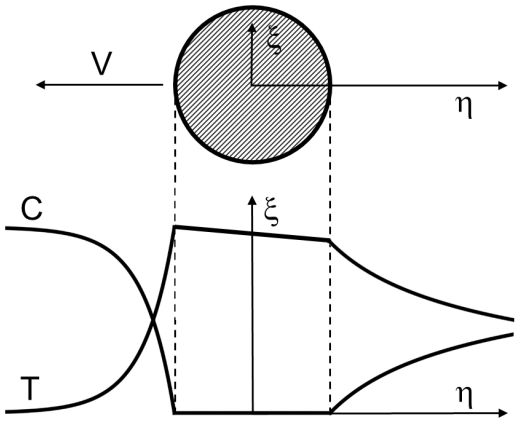

Figure 7. Up: Top sketch view of the flamelet in a plane parallel both to the paper and to the plates of the Hele–Shaw cell. Down: Profiles of temperature, T, and concentration, C, through the center of the flame ball.

There, the interior of the flame ball covers the interval $-R < \eta < R$. In the expansion (15), we will keep only the leading-order terms corresponding to $m = 0$. More-

over, we will set $\theta = 0$ for $\eta > 0$ and $\theta = \pi$ for $\eta < 0$. Conditions (10)–(14) on the flame ball interface $\eta = \pm R$ and $\eta = \pm\infty$ thus become

$$[S]_-^+ = 0,\ \Theta^{(0)} = 1, \tag{16}$$

$$\left[\frac{\partial\Theta^{(0)}}{\partial\eta}\right]_-^+ + \exp\left(\frac{S}{2}\right) = 0, \tag{17}$$

$$\left[\frac{\partial S}{\partial\eta}\right]_-^+ = \alpha\left[\frac{\partial\Theta^{(0)}}{\partial\eta}\right]_-^+, \tag{18}$$

$$\Theta^{(0)}(\eta = \pm\infty) = 0,\ S(\eta = \pm\infty) = 0. \tag{19}$$

and

$$C(-R < \eta < R) = 0. \tag{20}$$

the leading-order approximation $\beta \gg 1$,

$$\Theta^{(0)}(\eta > R) = \exp\left[k(\eta - R)\right]\frac{K_0(k\eta)}{K_0(kR)}, \tag{21}$$

$$\Theta^{(0)}(\eta < -R) = \exp\left[k(\eta + R)\right]\frac{K_0(-k\eta)}{K_0(kR)}, \tag{22}$$

$$\Theta^{(0)}(-R < \eta < R) = 1, \tag{23}$$

$$C^{(0)}(\eta) = 1 - \Theta^{(0)}(\eta). \tag{24}$$

the higher-order uniform approximation needed for the evaluation of $S = (\Theta + C - 1)\beta$,

$$\Theta(\eta > R) = \left[1 + \beta^{-1}S(R)\right]\cdot \exp\left[k(\eta - R)\right]\frac{K_0\left((k^2+q)^{\frac{1}{2}}\eta\right)}{K_0\left((k^2+q)^{\frac{1}{2}}R\right)}, \tag{25}$$

$$\Theta(\eta < -R) = \left[1 + \beta^{-1}S(-R)\right]\cdot \exp\left[k(\eta + R)\right]\frac{K_0\left(-(k^2+q)^{\frac{1}{2}}\eta\right)}{K_0\left((k^2+q)^{\frac{1}{2}}R\right)}, \tag{26}$$

$$\Theta(-R < \eta < R) = 1 + \beta^{-1}S(-R < \eta < R), \tag{27}$$

$$S(-R < \eta < R) = A + B\exp(k\eta)I_0(k|\eta|) - \nu\eta/2k, \tag{28}$$

where

$$A = [S(R) + S(-R)] - \frac{1}{2}BI_0(kR)[\exp(kR) + \exp(-kR)] \tag{29}$$

$$B = \frac{\nu R + S(R) - S(-R)}{kI_0(kR)[\exp(kR) - \exp(-kR)]}, \tag{30}$$

$$C(\eta > R) = 1 - \exp\left[kLe(\eta - R)\right]\frac{K_0(kLe\eta)}{K_0(kLeR)}, \tag{31}$$

$$C(\eta < -R) = 1 - \exp\left[kLe(\eta + R)\right]\frac{K_0(-kLe\eta)}{K_0(kLeR)}, \tag{32}$$

$$C(-R < \eta < R) = 0. \tag{33}$$

The uniform approximation employed in the above equations allows for meeting the boundary conditions $\Theta(\eta \to \infty) = 0$, $S(\eta \to \infty) = 0$ behind the self-drifting flamelet, where $\eta \sim \beta$.

4.2. Results

Equations (21)–(33) meet the continuity conditions (16) at $\eta = \pm R$. By substituting Equations (21)–(33) into jump conditions (17) and (18), one ends up with four algebraic relations for four unknown parameters $V = 2k$, R, $S(R)$, and $S(-R)$ as functions of the Lewis number parameter α, the re-scaled heat loss ν, and the Zeldovich number β (Figures 8–10). More technical details and the numerical procedure employed for the emerging algebraic problem are presented in the earlier version of the paper [16].

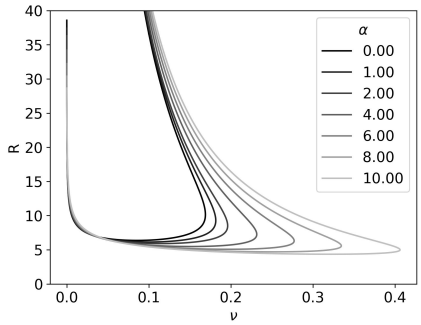

Figure 8. Locus of the flamelet radii, R, as a function of the heat loss, ν, for different Lewis number parameters, α.

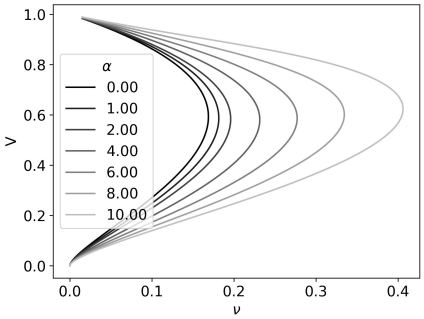

Figure 9. Locus of the velocities, V, as a function of the heat loss, ν , for different Lewis number parameters, α.

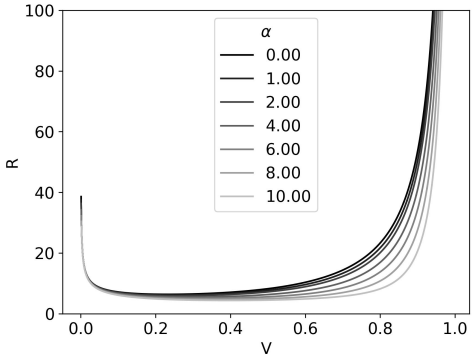

Figure 10. Locus of the dimensionless flamelet radii, R, as a function of dimensionless velocity, V, for different Lewis number parameters, α.

One can draw several conclusions from the results obtained.

1. The Lewis number parameter, α, strongly affects $V(\nu)$, $R(\nu)$ dependencies. The heat loss intensity at the quenching (turning) point, ν_q, increases with the decrease in the Lewis number, $Le \simeq 1 - \alpha/\beta$.
2. For re-scaled heat losses ν smaller than the heat loss intensity at the quenching point ν_q, $\nu < \nu_q$, multiplicity in the solutions $V(\nu)$, $R(\nu)$ is observed. A similar non-uniqueness is known to occur in planar ($R = \infty$) non-adiabatic flames, which leads to the α-independent relation between V and ν, $V^2 \ln(1/V) = \nu$ [17].
3. Once the solutions for $V(\nu)$, $R(\nu)$ for a certain Lewis number parameter α are available, one can plot spatial profiles of all state variables involved. For brevity, we depict here only the re-scaled temperature $\Theta(\eta)$ for the upper and lower branches of $V(\eta)$ (Figures 11 and 12). A significant drop in temperature Θ at the rear side ($\eta = R$) of the self-drifting flame ball might explain the horseshoe shape of the advancing flamelet. The latter is often perceived as a local extinction (opening) of the front.

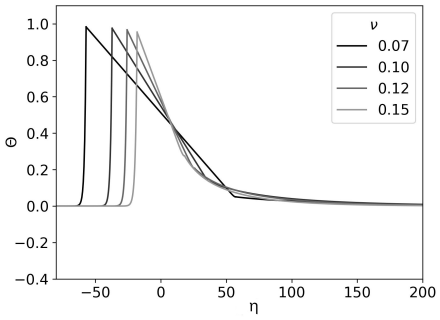

Figure 11. Profiles of the dimensionless re-scaled temperature, Θ, for Lewis number parameter $\alpha = 1$ and Zeldovich number $\beta = 10$ for different values of the re-scaled heat losses, ν, for the upper branch of $V(\nu)$. Longitudinal cut at the axis of the flamelet, $\xi = 0$.

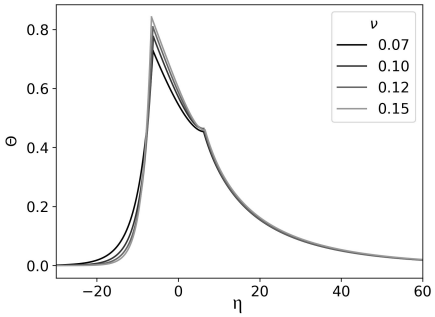

Figure 12. Profiles of the dimensionless re-scaled temperature, Θ, for Lewis number parameter $\alpha = 1$ and Zeldovich number $\beta = 10$ for different values of the re-scaled heat losses, ν, for the lower branch of $V(\nu)$. Longitudinal cut at the axis of the flamelet, $\xi = 0$.

5. Concluding Remarks

1. In constructing a workable approximate solution, we truncated a series involving an infinite number of terms, as in Equation (15), setting index m to zero to deal with sums involving only a finite number of terms.
2. There is an important distinction between the 3D and effectively 2D situation typical of large-aspect-ratio Hele–Shaw cells. The 3D case allows for stationary spherical flame balls which may bifurcate into a self-drifting mode [11,12]. In the 2D case, the non-drifting circular flame balls are ruled out. They cannot meet boundary conditions at infinity (due to the logarithmic tail of the associated concentration profiles [8]). So, in narrow gaps, 2D self-drifting flame balls should emerge not as a bifurcation but rather as the only way for the 2D flame balls to exist.

3. In the present study, the pattern of flame disintegration is controlled by heat loss intensity $q = (\pi \ell_{th}/d)^2$, which in turn may be controlled by the width of the Hele–Shaw gap (d) or the mixture composition (% H_2 or ℓ_{th}) [4,10,18].
4. The reaction diffusion model in Section 2 does not seem capable of reproducing two-headed flamelets. The latter is often observed experimentally [4,19] as well as in simulations of more sophisticated models that consider the burned gas thermal expansion [8,20] and are therefore susceptible to Darrieus–Landau instability. At the moment, the issue of two-headed flamelets remains unexplained.
5. This study is devoted to estimates of the propagation velocity of an individual flame ball in a flat channel. It would be interesting to extend the analysis over the collective propagation of a group of flame balls appearing in Figures 1–3, where the flamelets are competing for common fuel and mutual heating of one another. A mean-field type of approach such as that developed by D'Angelo and Joulin [21] or Williams and Grcar [22] seems particularly promising.
6. In the present study, flame balls emerge in gaseous premixtures as an extreme case of diffusive thermal instability, where invariably $Le < 1$. A similar pattern is observed in the smoldering burning of thin solid sheets with and without imposed air flows [23–29]. There, similar to the gaseous systems, the effective Lewis number is considerably below unity [29]. It would be interesting to also extend the 1D approach of this paper to the smoldering problem.

Author Contributions: Conceptualization, M.K. and G.S.; Software, J.Y. and L.K.; Formal analysis, J.Y. and G.S.; Investigation, M.K.; Writing—original draft, J.Y. and G.S.; Writing—review & editing, L.K. and M.K.; Visualization, J.Y.; Supervision, M.K. and G.S. All authors have read and agreed to the published version of the manuscript.

Funding: This research was supported in part by the US-Israel Binational Science Foundation (grant 2020-005).

Data Availability Statement: The original contributions presented in this study are included in the article. Further inquiries can be directed to the corresponding author.

Conflicts of Interest: The authors declare that they have no known competing financial interests or personal relationships that could have appeared to influence the work reported in this paper.

References

1. Tingas, E.-A.; Taylor, A.M.K.P. *Hydrogen for Future Thermal Engines*; Springer: Berlin/Heidelberg, Germany, 2023.
2. Williams, F.A. *Combustion Theory*; Perseus Book Pub.: Reading, MA. USA, 1985.
3. Clavin, P.; Searby, G. *Combustion Waves and Fronts in Flows: Flames, Shocks, Detonations, Ablation Fronts and Explosion of Stars*; Cambridge University Press: Cambridge, UK, 2016.
4. Veiga-López, F.; Kuznetsov, M.; Martínez-Ruiz, D.; Fernández-Tarrazo, E.; Grune, J.; Sánchez-Sanz, M. Unexpected propagation of ultra-lean hydrogen flames in narrow gaps. *Phys. Rev. Lett.* **2020**, *124*, 174501. [CrossRef]
5. Veiga-López, F.; Martínez-Ruiz, D.; Kuznetsov, M.; Sánchez-Sanz, M. Thermoacoustic analysis of lean premixed hydrogen flames in narrow vertical channels. *Fuel* **2020**, *278*, 118212. [CrossRef]
6. Kuznetsov, M.; Grune, J. Experiments on combustion regimes for hydrogen/air mixtures in a thin layer geometry. *Int. J. Hydrogen Energy* **2019**, *44*, 8727–8742. [CrossRef]
7. Kagan, L.; Sivashinsky, G. Self-fragmentation of nonadiabatic cellular flames. *Combust. Flame* **1997**, *108*, 220–226. [CrossRef]
8. Martínez-Ruiz, D.; Veiga-López, F.; Fernández-Galisteo, D.; Kurdyumov, V.N.; Sxaxnchez-Sanz, M. The role of conductive heat losses on the formation of isolated flame cells in Hele-Shaw chambers. *Combust. Flame* **2019**, *209*, 187–199. [CrossRef]
9. Dejoan, A.; Fernández-Galisteo, D.; Kurdyumov, V.N. Numerical study of the propagation patterns of lean hydrogen-air flames under confinement. In Proceedings of the 29th ICDERS, SNU, Siheung, Republic of Korea, 23–28 July 2023.
10. Kuznetsov, M.; Yanez, J.; Veiga-López, F. Near limit flame propagation in a thin layer geometry at low Peclet numbers. In Proceedings of the 18th International Conference on Flow Dynamics (ICFD 2021), Miyagi, Japan, 27–29 October 2021; pp. 688–692.
11. Brailovsky, I.; Sivashinsky, G. On stationary and travelling flame balls. *Combust. Flame* **1997**, *110*, 524–529. [CrossRef]

12. Minaev, S.; Kagan, L.; Joulin, G.; Sivashinsky, G. On self-drifting flame balls. *Combust. Theor. Model.* **2001**, *5*, 609. [CrossRef]
13. Matkowsky, B.; Sivashinsky, G. An asymptotic derivation of two models in flame theory associated with the constant density approximation. *SIAM J. App. Math.* **1979**, *37*, 686–699. [CrossRef]
14. Lamb, H. *Hydrodynamics*; Cambridge University Press: Cambridge, UK, 1924.
15. Tomotika, S.; Aoi, T. The steady flow of viscous fluid past a sphere and circular cylinder at small Reynolds numbers. *Q. J. Mech. Appl. Math.* **1950**, *3*, 141–161. [CrossRef]
16. Yanez, J.; Kagan, L.; Sivashinsky, G.; Kuznetsov, M. Modeling of 2D self-drifting flame-balls in Hele-Shaw cells. *Combust. Flame* **2023**, *258*, 113059. [CrossRef]
17. Sivashinsky, G.; Matkowsky, B. On the stability of nonadiabatic flames. *SIAM J. Appl. Math.* **1981**, *40*, 255–260. [CrossRef]
18. Moskalev, P.V.; Denisenko, V.P.; Kirillov, I.A. Classification and dynamics of ultralean hydrogen–air flames in horizontal cylindrical Hele–Shaw cells. *J. Exp. Theor. Phys.* **2023**, *137*, 104–113. [CrossRef]
19. Escanciano, J.Y.; Kuznetsov, M.; Veiga-López, F. Characterization of unconventional hydrogen flame propagation in narrow gaps. *Phys. Rev. E* **2021**, *103*, 033101. [CrossRef]
20. Domínguez-González, A.; Martínez-Ruiz, D.; Sánchez-Sanz, M. Stable circular and double-cell lean hydrogen-air premixed flames in quasi twodimensional channels. *Proc. Combust. Inst.* **2023**, *39*, 1731–1741. [CrossRef]
21. D'Angelo, Y.; Joulin, G. Collective effects and dynamics of non-adiabatic flame balls. *Combust. Theory Model.* **2001**, *5*, 1–20. [CrossRef]
22. Williams, F.A.; Grcar, J.F. A hypothetical burning velocity formula for very lean hydrogen–air mixtures. *Proc. Combust. Inst.* **2009**, *32*, 1351–1357. [CrossRef]
23. Zhang, Y.; Ronney, P.; Roegner, E.; Greenberg, J. Lewis number effects on flame spreading over thin solid fuels. *Combust. Flame* **1992**, *90*, 71–83. [CrossRef]
24. Zik, O.; Olami, Z.; Moses, E. Fingering instability in combustion. *Phys. Rev. Lett.* **1998**, *81*, 3868. [CrossRef]
25. Matsuoka, T.; Nakashima, K.; Nakamura, Y.; Noda, S. Appearance of flamelets spreading over thermally thick fuel. *Proc. Combust. Inst.* **2017**, *36*, 3019–3026. [CrossRef]
26. Zhu, F.; Lu, Z.; Wang, S.; Yin, Y. Microgravity diffusion flame spread over a thick solid in step-changed low velocity opposed flows. *Combust. Flame* **2019**, *205*, 55–67. [CrossRef]
27. Malchi, J.; Yetter, R.; Son, S.; Risha, G. Nano-aluminum flame spread with fingering combustion instabilities. *Proc. Combust. Inst.* **2007**, *31*, 2617–2624. [CrossRef]
28. Olson, S.; Baum, H.; Kashiwagi, T. Finger-like smoldering over thin cellulosic sheets in microgravity. *Symp. (Int.) Combust.* **1998**, *27*, 2525–2533. [CrossRef]
29. Uchida, Y.; Kuwana, K.; Kushida, G. Experimental val idation of Lewis number and convection effects on the smoldering combustion of a thin solid in a narrow space. *Combust. Flame* **2015**, *162*, 1957–1963. [CrossRef]